

Kai Germer*
Juergen Braun



Laboratory experiments were conducted to assess the role of water table position and pore water pressure variation on natural slope stability. Slope failures were found to be preceded by an abrupt decrease in pore water pressure. We suggest that slope stability assessment requires real-time monitoring of pore water pressure variation.

K. Germer and J. Braun, Univ. of Stuttgart, Institute of Hydraulic Engineering, Research Facility for Subsurface Remediation-VEGAS, Pfaffenwaldring 61, 70569 Stuttgart, Germany. *Corresponding author (kai.germer@iws.uni-stuttgart.de).

Vadose Zone J. 10:477–486
doi:10.2136/vzj2009.0154
Received 30 Oct. 2009.
Posted online 20 Jan. 2011.

© Soil Science Society of America
5585 Guilford Rd., Madison, WI 53711 USA.
All rights reserved. No part of this periodical may be reproduced or transmitted in any form or by any means, electronic or mechanical, including photocopying, recording, or any information storage and retrieval system, without permission in writing from the publisher.

Effects of Saturation on Slope Stability: Laboratory Experiments Utilizing External Load

Failure of natural slopes may result in considerable damage to both human health and real estate properties. The conditions “necessary” for a slope to fail have been investigated thoroughly in the past. Additional work is still necessary regarding the causes that trigger a slope to move and that may in the long run even be helpful to predict the failure of a slope. We conducted experiments to investigate the influence of various groundwater conditions on slope stability. Our results showed that the position of the groundwater table and especially a variation in pore water pressure greatly affect the slope stability under loaded conditions. Moreover the results showed that slope failures are preceded by an abrupt decrease in pore water pressure. We suggest that a monitoring of the fluctuation of pore water pressure in a real slope may give an indication of its inherent stability.

Failure of natural slopes may lead to catastrophic consequences for the population, the environment, and nature. Slope movement or a sudden slope failure often occurs due to heavy rainfall following a long-lasting creeping caused by a weakening of shear zones. Interflow, infiltration, and groundwater flow as well as evaporation contribute, to a very different extent and on very different space and time scales, to elastic and visco-plastic soil deformation. The interaction of hydrologic, subsurface hydraulic, and soil mechanical processes across a large range of scales is being investigated by an interdisciplinary research project established in January 2006. This research group combines numerical models and experimental investigations to gain a better understanding of the mechanisms that trigger this slope movement and to assess whether this movement might eventually cause a slope failure. The approach of the research is to combine improved process models with coupling, averaging, and upscaling processes on the one hand and with improved experimental methods on the other. The tools to be developed will need to be verified based on controlled experiments in the laboratory before being transferred to larger scales. Therefore, benchmark experiments to investigate shear failure need to be conducted to increase the understanding of processes leading to slope failure with an eye on the real slope situation and to provide data sets for the verification of numerical models.

The Heumöser, a large hillslope located in the proximity of the town of Ebnit, Vorarlberg, Austria, has been known to move slowly for the last decades (Lindenmaier et al., 2005; Wienhöfer et al., 2009). It has been postulated that macropores in the upper reaches of the slope favor rapid infiltration, causing a rapid increase in water pressure in the underlying highly permeable strata. This increased water pressure leads to an increase in buoyancy forces at the bottom of the slope, which in turn causes destabilization and a subsequent increase in slope movement velocity. The investigation of this hypothesis is one goal of the interdisciplinary research project mentioned above. Our experiments were performed to increase the understanding of the physical processes involved and to provide data to verify numerical models.

An artificial slope was set up with clearly defined boundary and initial conditions. An external load was applied on the slope as a boundary condition to account for the uphill extension of a natural slope. Then either the external load on the slope or the water saturation in the porous medium was varied until slope failure occurred. Hence, the effects of these parameters could be assessed. The data were shared with other project partners in order for them to verify their numerical models (Ehlers et al., 2011).

It needs to be pointed out that the results of this work cannot be directly applied to the prediction of failure of a natural slope. The experiments were performed using homogeneous sand packing, while a natural slope consists of heterogeneous, anisotropic soils of variable permeabilities. Saturation in the experiments could be deduced from capillary pressure data and the capillary–pressure saturation curves determined before conducting the actual experiments. Knowledge regarding saturation in the field is unavailable in such detail. Moreover, due to the size of the experiment and the grain size distribution of the sand used, most of the experimental setup was at or close to full saturation, independent of the location of the water table.

Nevertheless, these experiments can contribute significantly to an understanding of the dependence of slope stability on external load and pore water pressure. Additionally, their use in the verification of numerical models will contribute to eventually bridge the gap from the laboratory to an actual field site.

An overview of the literature from the different disciplines investigating rainfall-induced natural landslides was given by Crosta and Frattini (2008). Investigations have ranged from large-scale field monitoring systems using remote sensing methods to landslide modeling at different scales. Field investigations of rainfall-induced slope failure focused on the interrelation between infiltration and pore water pressure were conducted by Tsaparas et al. (2003) and Rahardjo et al. (2005).

While these studies reported on field experiments, our study focused on slope failure experiments at the laboratory scale. In the literature, some experimental studies of slope failure in boxes, containers, tanks, or flumes have been described. Most of these experiments had a focus on debris or mass flow failures caused by erosion and liquefaction triggered by rainfall (Iverson et al., 1997, 2000; Wang and Sassa, 2001, 2003; Okura et al., 2002; Moriwaki et al., 2004; Lourenco et al., 2006; Olivares and Damiano, 2007; Tohari et al., 2007; Wang and Shibata, 2007; Huang et al., 2008, 2009). All of these studies worked without external loads. They included different pore water pressures, matric suctions, or soil moisture measurements and investigated different failure patterns and changes in pore water pressure during failure. Iverson et al. (2000) focused in their experiments on landslides triggered by rising pore water pressures under different soil porosities. Moriwaki et al. (2004), using a 21.6-m-long inclined flume to minimize scale effects, investigated pore water pressure behavior at failures under high saturation triggered by rainfall and determined the pore water pressure decrease and increase effects during the failure phase.

Few studies have concentrated on slope destabilization by an increase of groundwater flow or upward water injection in model slopes. Lourenço et al. (2006) observed pore water generation in sandy slopes consisting of different layers after sprinkling water on

the surface or upward groundwater injection until seepage erosion and retrogressive slides occurred.

Some experiments with external loads can be found in research on mechanical reinforcement of embankments. Experiments at the meter scale with strip footing as an external load placed on embankment crests were conducted by Huang et al. (1994), Yoo (2001), Bathurst et al. (2003), and El Sawwaf (2007). These researchers focused on a comparison of reinforced and unreinforced embankments. They found methods to stabilize slopes through differently arranged layered or striped reinforcement elements. These studies, however, concentrated on the load displacement behavior of a slope and did not focus on the pore water pressure or matric suction effects in the slope body. External load experiments in a sand box were performed by Roy and Mandal (2009). They focused on different positions of a load realized as a rigid block on top of the slope and investigated the dependencies of the slope angle and the anisotropic layering of the slope body. Their results showed different compaction and failure phases during the progressive indentation due to the external load.

A study by Cho and Lee (2001) examined stability and calculated safety factors for an unsaturated slope using numerical tools. Simulated rainwater infiltration into different permeable materials of the slope body led to a change in matric suction and thus a change in the stress fields that consequently affected the slope stability. Paul and Kumar (1997) developed a computer program to analyze the stability of slopes with building loads. Some other finite element computations for slope stability problems were performed by Laouafa and Darve (2002), Li et al. (2003), and Ehlers et al. (2004). Li et al. (2003) showed, among others, a numerical example for a 19.2-m-long and 9.6-m-high slope body loaded by a footing on its crest. They compared low and high loading rates and worked out excess pore pressure and equivalent plastic strain distributions in the shear band area by considering dynamic effects.

♦ Materials and Methods

The experiments were performed at the Research Facility for Subsurface Remediation (VEGAS) at the University of Stuttgart, Stuttgart, Germany. Our hypothesis was that slope failure might be triggered by (rapidly) changing water content. We focused therefore on three sets of experiments. In the first two sets, different groundwater situations were established (static and steady flow, respectively) before a stepwise increase of the external load until slope failure occurred. The primary goal of these first two experiments was to determine suitable initial conditions to then test the hypothesis in a third set of experiments. The load applied was meant to represent an upslope extension of the experiment and was selected such that the slope was stable at low water contents but would become unstable at higher water contents. In the third set of experiments, starting with an initially static groundwater level, the slope was preloaded to $\sim 90\%$ of the expected maximum

supported load determined in the first set of experiments with static groundwater. Then water was injected in the vicinity of the footslope, resulting in a local increase in pore water pressure and subsequent slope failure. The experiments were monitored extensively to provide insight into the behavior of a slope and an extensive data set to validate numerical models.

The experimental flume (Fig. 1 and 2) was 100 cm high, 200 cm long, and 80 cm wide and was built of steel (Germer and Braun, 2009). The size of the flume, the dimensions of the walls and supporting beams, as well as the shape (height and inclination) of the slope body were based on preliminary numerical calculations. One long side of this flume was a glass pane to allow visual observation of water saturation and soil deformation. Its opposite side was constructed of steel and fitted with piezometer holes along the bottom. Each piezometer hole was covered with a fine stainless steel mesh and connected to a pressure transducer. Both narrow sides were constructed as “wells” to establish constant-head boundary conditions, and subsequently flow, if so desired. Technically, these wells were made of a perforated metal plate covered with fine-screen stainless steel mesh installed at a 10-cm distance from the wall of the flume. The wells were connected to constant-head tanks and fitted with pressure transducers. The bottom of the flume was a steel plate and the top was open to atmosphere.

The external load, simulating the upper reaches of the slope, could be applied via a horizontally placed pressure plate (30 by 78 cm), which could be pressed into the top of the slope via double-acting hydraulic cylinders. The upper end of the hydraulic cylinders could be moved horizontally via a linear induction motor to ensure that the force applied to the pressure plate acted in the vertical direction, independent of the horizontal displacement of the pressure plate. Ultrasonic distance sensors not only controlled the linear induction motor, they also measured and monitored the horizontal and vertical movement of the plate as well as its incline during the experiment.

The voltage signals from the ultrasonic sensors and from the pressure transducers were logged using a USB LabJack UE9 data acquisition device (LabJack Corp., Lakewood, CO). The continuous processing of the data was done with ProfiLab 3.0 software (Abacom Ingenieurgesellschaft, Ganderkesee, Germany). This software was also used to continuously analyze the ultrasonic sensor measurements and, based on those measurements, to automatically adjust the vertical alignment of the hydraulic cylinders.

The porous medium used for all experiments was a fine sand (GEBA, Dorfner, Hirschau, Germany) with grain sizes ranging from 0.03 to 0.3 mm (Fig. 3). With a 10% sieve retention diameter (d_{10}) of 0.09 mm and a 60% retention diameter (d_{60}) of 0.11 mm, the sand had a coefficient of uniformity (Cu) of 1.2, indicating a very uniform porous medium. The flume was packed wet, i.e., before a layer was laid, the water level was raised to ensure 2 to 3 cm of ponded water. The height of each layer was around 5 cm and

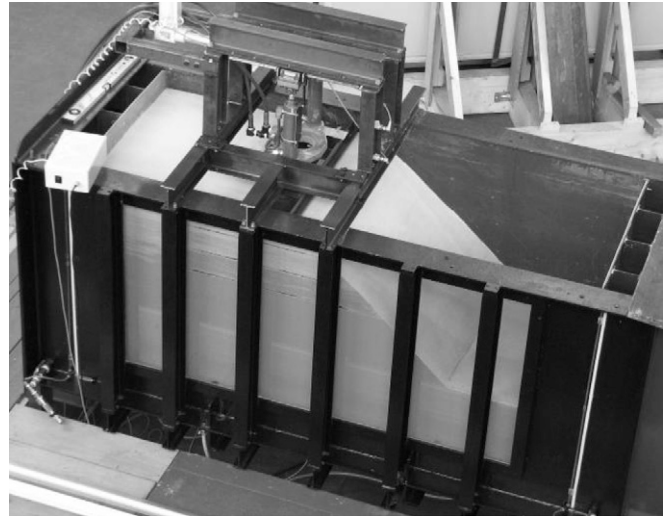


Fig. 1. Laboratory flume for slope failure experiments, including setup to impose external load.

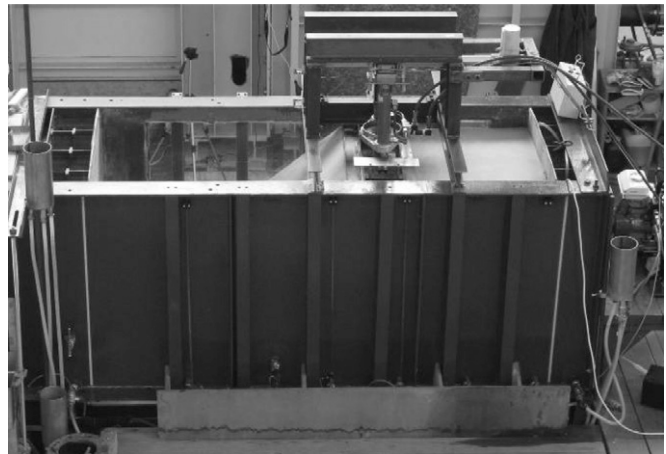


Fig. 2. Rear view of flume with constant-head tanks and pressure transducers.

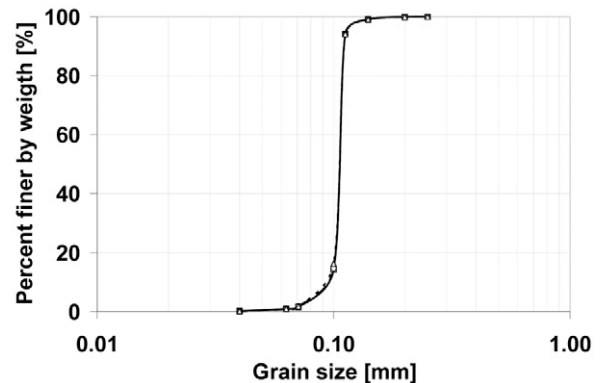


Fig. 3. Grain size distribution of the fine sand determined on three samples.

after placing the sand, it was compacted with a board of nails (10 by 20 cm). The target bulk density was 1.5 to 1.55 g/cm³. Once the whole flume was filled to a height of 90 cm, the water was

drained and the soil material on one side was dug out to obtain the shape of the slope with an angle of 40° . During the sand removal, four samples were taken at each depth of 20 and 40 cm below the ground surface and a bulk density ranging from 1.50 to 1.56 g/cm³ was confirmed at these depths.

While in the saturated zone the water tends to decrease the slope stability, the capillary forces acting in the unsaturated zone may help stabilize the slope. The magnitude of the capillary forces is a function of saturation and the soil parameters and needs to be established experimentally. Two methods were used to accomplish this. First, we used a controlled outflow cell (Lorentz et al., 1992). In this method, a cylindrical sample with a diameter of 5.2 cm and a height of 3 cm is drained stepwise over a 50-kPa high-flow ceramic plate (Soilmoisture Equipment Corp., Goleta, CA). Once equilibrium was reached between the water and the air pressure, the capillary pressure was determined and paired with the corresponding water saturation (determined from the amount of water drained). Second, a multistep outflow–inflow method (Zurmühl, 1996, 1998) combined with the evaporation method of Peters and Durner (2008) was used to obtain additional information about imbibition and the hysteresis behavior of the sand. This investigation was conducted on soil cylinders with a diameter of 7.3 cm and a height of 9.4 cm as described in Ahrenholz et al. (2008). Soil parameters were determined by inverse parameter estimation (Durner et al., 1997), based on the unimodal constrained model of van Genuchten (1980). The van Genuchten parameters for the soil are shown in Table 1 for primary and secondary drainage as well as primary imbibition. The saturated hydraulic conductivity was measured to be 2.17×10^{-4} m/s. The capillary pressure–saturation curves for this sand are presented in Fig. 4.

Experimental Setup

As described above, the experiments were to fulfill three goals. The first set of experiments (Case A) was to determine the maximum uphill load the slope could sustain. The second set of experiments (Case B) was conducted to determine the minimum load under steady-state groundwater flow conditions and the third set (Case C) was to show if a dynamic change in the pore-water pressure could result in an even stronger decline in stability and, if possible, quantify this decrease in stability. To show that the results were

Table 1. Parameter of the fine sand measured with a Corey–Lorentz cell (CLC) and with the multistep outflow (MSO, draining) and multistep inflow (MSI, imbibing) methods.

| Experiment | Residual water content | Saturated water content | van Genuchten parameters | |
|----------------|------------------------|-------------------------|--------------------------|--------|
| | | | α | n |
| | | | 1/cm | |
| Draining CLC | 0.027 | 0.415 | 0.013 | 8.721 |
| Draining 1 MSO | 0.0712 | 0.402 | 0.0151 | 14.999 |
| Imbibing MSI | 0.0712 | 0.336 | 0.0574 | 2.589 |
| Draining 2 MSO | 0.0628 | 0.336 | 0.016 | 9.277 |

reproducible, multiple experiments were run for each case (five for Case A, three for Case B, and four for Case C). Packing data and boundary conditions for all experiments are listed in Table 2.

Case A: Static Groundwater, Low Groundwater Table

The constant water head boundaries (h_w) on both sides were set at left side $h_{wl} =$ right side $h_{wr} = 10$ cm (Fig. 5a) yielding, after drainage of the slope body had ceased, initial conditions of a static groundwater level 30 cm below the foot of the slope. Hence, the slope body (including the expected shear zone) was unsaturated and therefore capillary forces were acting to stabilize the slope (although it must be said that, due to the high capillary rise, these forces were not expected to be large).

The hydraulic boundary conditions were maintained constant throughout the experiment. The load on the pressure plate was increased stepwise ($\Delta q \sim 10$ kN/m²), and subsequent load increases were imposed once a distinct change of deformation had ceased. This stepwise increase of pressure was continued until the slope failed. The load and the corresponding displacement of the load plate were recorded. Additionally, pore water pressure readings throughout the experiment were monitored.

Case B: Steady-State Groundwater Flow, High Groundwater Table

In Case B (Fig. 5b) the constant-head boundaries were set at $h_{wl} = 70$ cm and $h_{wr} = 10$ cm. Therefore, after cessation of the drainage process, the initial conditions for the experiments consisted of steady-state groundwater flow from the left to the right. The constant-head boundaries were chosen such that the water table was close to the foot of the slope. Due to the slope of the groundwater table, a part of the expected shear plane was now under positive water pressure. Hence, no stabilizing capillary forces were expected in this region. Moreover, due to the high entry pressure of the sand, it was a good assumption that the whole experiment was virtually saturated. The hydraulic boundary conditions were maintained throughout the experiment. The external load was applied as described for Case A and the same parameters were monitored.

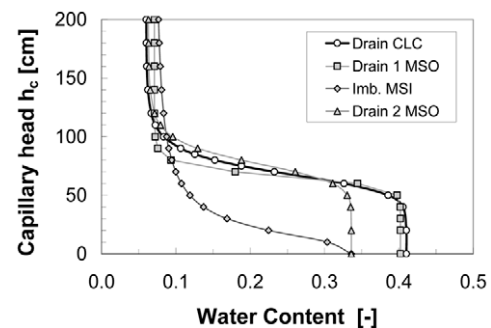


Fig. 4. Capillary head–water content curves for the fine sand measured with a Corey–Lorentz cell (CLC) and with the multistep outflow (MSO, draining) and multistep inflow (MSI, imbibing) methods.

Table 2. Packing parameters, initial conditions, and load (q) applied for Case C (q_{max}) as well the load at slope failure (q_f) for Cases A and B and displacement results.

| Case | Exp. | Bulk density g/cm ³ | Porosity | Head | | External load | | q_{max} | Max. vertical displacement mm | q_f |
|--------|------|-----------------------------------|----------|------|-------|---------------|-----------|-----------|----------------------------------|-------|
| | | | | Left | Right | Δq | Time step | | | |
| Case A | A1 | 1.53 | 0.42 | 10 | 10 | 7 | 2 | NA† | 11.9 | 235.6 |
| | A2 | 1.52 | 0.43 | 10 | 10 | 10 | 1 | NA | 12.1 | 237.7 |
| | A3 | 1.53 | 0.42 | 10 | 10 | 10 | 2 | NA | 10.0 | 242.0 |
| | A4 | 1.51 | 0.43 | 10 | 10 | 10 | 1 | NA | 8.6 | 224.0 |
| | A5 | 1.51 | 0.43 | 10 | 10 | 10 | 2 | NA | 11.9 | 242.5 |
| Mean | A | 1.52 | 0.43 | 10 | 10 | | | | 10.9 | 236 |
| Case B | B1 | 1.51 | 0.43 | 69 | 10 | 7 | 1 | NA | 13.6 | 190.2 |
| | B2 | 1.52 | 0.43 | 70 | 10 | 7 | 1 | NA | 16.2 | 196.0 |
| | B3 | 1.50 | 0.43 | 71 | 10 | 7 | 1 | NA | 15.6 | 188.9 |
| Mean | B | 1.51 | 0.43 | 70 | 10 | 7 | 1 | | 15.1 | 192 |
| Case C | C1 | 1.56 | 0.41 | 10 | 10 | 35 | 5 | 214.6 | 10.8 | NA |
| | C2 | 1.53 | 0.42 | 10 | 10 | 35 | 5 | 215.7 | 9.1 | NA |
| | C3 | 1.52 | 0.43 | 10 | 10 | 35 | 5 | 214.2 | 10.9 | NA |
| | C4 | 1.56 | 0.41 | 10 | 10 | 35 | 5 | 215.1 | 11.4 | NA |
| Mean | C | 1.54 | 0.42 | 10 | 10 | 35 | 5 | 215 | 10.6 | |

† Centimeters of water column.

‡ NA, not applicable.

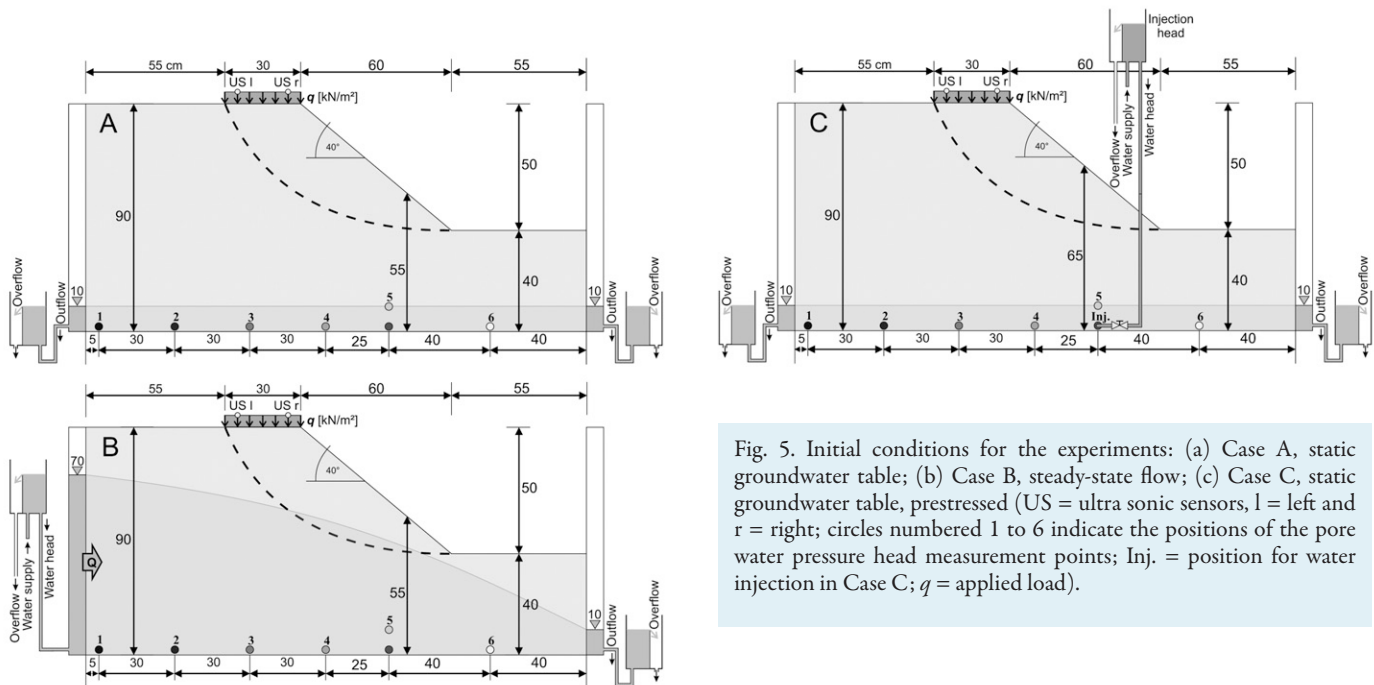


Fig. 5. Initial conditions for the experiments: (a) Case A, static groundwater table; (b) Case B, steady-state flow; (c) Case C, static groundwater table, prestressed (US = ultra sonic sensors, l = left and r = right; circles numbered 1 to 6 indicate the positions of the pore water pressure head measurement points; Inj. = position for water injection in Case C; q = applied load).

Case C: Transient Groundwater Flow, Initially Low Groundwater Table

In Case C (Fig. 5c), there was one change in the general experimental setup: a drainage pipe was embedded underneath the foot of the slope. This pipe was connected to a constant-head tank and allowed a rapid increase in water head at the bottom of the slope.

The initial hydraulic conditions were as described for Case A. In addition, there was an initial external load of 215 kN/m² (corresponding to 91% of the average maximum load sustained in Case A). This initial load was imposed as described for the other cases; however, the increase ceased at a predetermined upper limit rather than at slope failure.

The initial conditions were sustained as boundary conditions throughout the experiment. As an additional boundary condition, a constant head of 125 cm was instantaneously applied to the drainage pipe, resulting in a transient increase in head and, hence, flow locally underneath the foot of the slope.

In addition to the parameters mentioned for Cases A and B, the pressure in the drainage pipe was monitored.

Results

The experiments of Cases A and B, static and steady-state groundwater, respectively, can be divided into three time phases. In the first phase, the pore water pressure (heads 1–6) readings were nearly stable. The slope, while being stable, showed a slight deformation due to the stepwise increase in the load. In the second phase, the pore water pressures showed a distinct decrease, accompanied by a slightly accelerated deformation of the slope, while the pressure on the load remained constant or even increased. This phase ended with the structural failure of the slope. The third phase was initiated by the actual slope failure and included the subsequent changes in the pore water pressure. Once these water pressures had reached constant values, static or steady-state conditions prevailed again in the water. Figure 6 shows a typical picture of a failed slope with a clearly distinguished shear zone.

The main results for each experiment are listed in Table 2. In Fig. 7a to 7c, one experiment for each case is shown to exemplify the distinct features of the respective cases. Note that the time scale in Fig. 7 has been exaggerated at the later time interval.

For Case A, the experiments were packed at an average bulk density $\rho_b = 1.52 \text{ g/cm}^3$ with an average porosity of $\Phi = 0.43$. The external load was applied following various schemes including a continuous



Fig. 6. Slope body and shear plane after failure. The actual measurements of this specific demonstration experiment were not used in the evaluation because the colored sand slightly changed its behavior.

stepwise increase (10 kN/m^2 every 2 min), a rapid initial increase followed by slower subsequent increases, and continuous stepwise increases interrupted by longer periods at constant pressures to allow a cessation of the deformation. While the load was being applied, both the vertical displacement of the pressure plate and its inclination were measured.

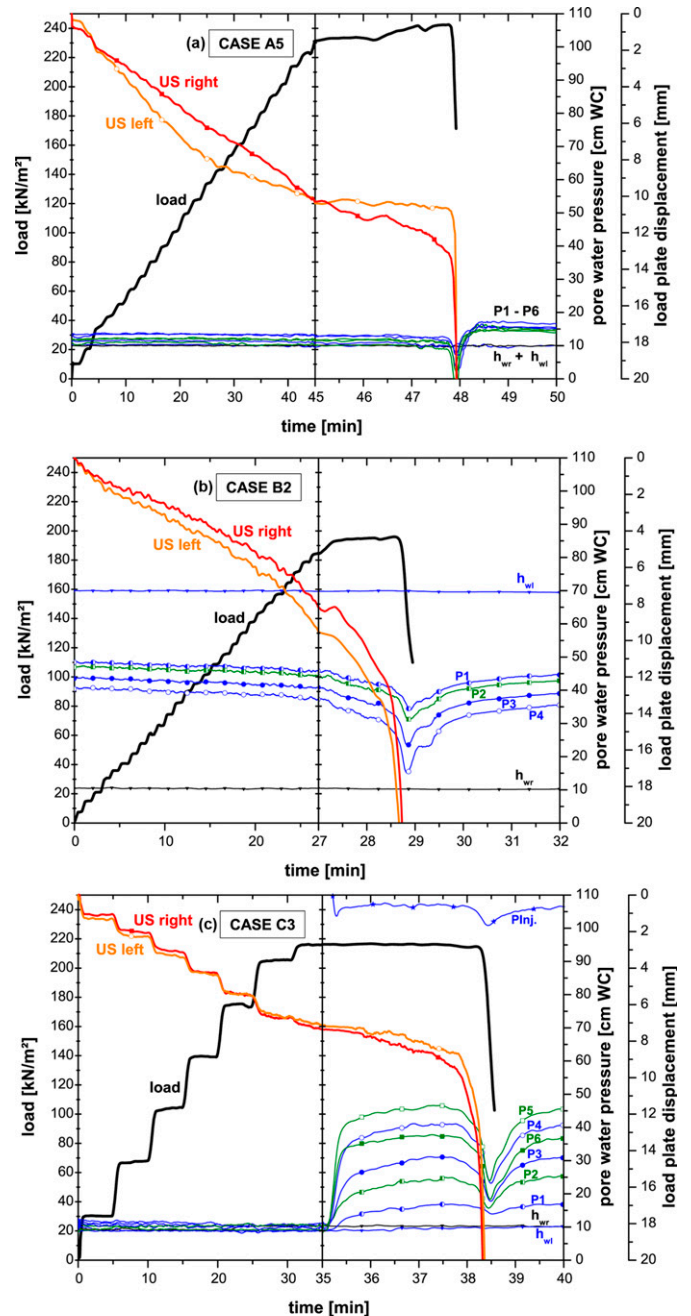


Fig. 7. Load, heads, and compaction in the system for Experiments (a) A5, (b) B2, and (c) C3, where US left and right depict the readings from the ultrasonic sensor, h_{wl} and h_{wr} are the left and right constant-head boundary conditions; P1 to P6 are the pore water pressure and PInj is the injection pressure, each in centimeters of water column (cm WC).

The maximum sustainable load or failure load, q_f , ranged from 224 to 243 kN/m² with a mean q_f of 236 kN/m² and a standard deviation of 7.5 kN/m². No direct correlation either with bulk density or with the way the load was applied could be detected. Therefore, in all subsequent experiments (Cases B and C), the load was applied stepwise.

Figure 7a shows as an example the results for Case A5. The load was increased stepwise ($\Delta q \sim 10$ kN/m² at each ~ 2 -min step) for 48 min until the slope failed at a load of approximately $q_f = 243$ kN/m². It can be seen that each increase in load resulted in a rapid deformation (compaction) of the soil. These deformations were very small (~ 0.5 mm), however, and they nearly ceases after each 2-min time interval chosen for the stepwise load increase. The maximum load (q_f) yielded a deformation of 12 mm (vertical displacement). The maximum inclination of the load plate (differences between the left-hand side and the right-hand side divided by the width of the plate) was < 0.005 and, hence, may be neglected. Looking at the pore water pressure heads, it may be observed that the heads in the system were stable, indicating that the compaction was slow enough to allow a redistribution of the water. Around the time of failure, however, a sharp decrease in head was observed. This may be attributed to a sudden increase in porosity due to a sudden decrease in compaction while the slope failed.

For Case B, the average packing density was $\rho_b = 1.51$ g/cm³ with an average porosity of $\Phi = 0.43$. The external load was increased stepwise ($\Delta q \sim 5$ kN/m², time step $\Delta t \sim 1$ min). Figure 7b shows an example of the experiments conducted for Case B, i.e., a system with steady-state groundwater movement. For all experiments of Case B, the head on the inflow side, h_{wp} , was fixed at 70 cm. The hydraulic head at the first piezometer (5 cm inside the sand body from the left), however, showed a large drop in water head (of ~ 20 –25 cm). It has to be concluded that there was a significant head loss in the wire mesh of the well and, hence, as a boundary condition, the reading of the first piezometer should be used rather than the water level in the well.

In the experiments for Case B, the slope failed on average at $q_f \sim 192$ kN/m², or at $\sim 81\%$ of the sustainable load determined for Case A (for detailed values, see Table 2).

Deformations for the system were similar to the deformations in Case A; however, the failure was not as sudden. Figure 7b clearly shows that the deformation increased for a nearly 1 min before the slope failed. The pore water pressure at each piezometer slowly decreased throughout the initial phase of the experiment and showed, minutes before failure, a more rapid decrease accompanied by a slight increase in the vertical displacement of the pressure plate. As for the vertical displacement, this decrease in water pressure was less rapid than the one observed for Case A.

Comparing the load-displacement relationship of Case A and Case B (Fig. 8), it can be stated that increasing the water saturation and thus decreasing the capillary suction in the vicinity of the shear plane hardly had any effect on the load–deformation relationship of the respective systems. It did, however, greatly affect the stability of the system. In the Case B experiments, a decrease in slope stability of 19% in comparison to Case A was observed.

For Case C, the average packing density was $\rho_b = 1.54$ g/cm³ with a corresponding average porosity of $\Phi = 0.42$ (Table 2). The initial hydraulic conditions were the same as in Case A (static groundwater with a groundwater table ~ 30 cm below the foot of the slope). The external load was increased stepwise ($\Delta q \sim 35$ kN/m², $\Delta t \sim 5$ min) but was limited to $q_{max} = 215$ kN/m². Case C (Fig. 7c) experienced a somewhat slower load–displacement relationship than Case A. Similarly to Case A, the pore water pressure was not affected by the compaction, indicating that the increase in load and the corresponding compaction were slow enough to allow the water pressure to equilibrate. At time $t = 35$ min, the boundary condition in the injection pipe underneath the foot of the slope was instantaneously increased to 125 cm, resulting in an instantaneous increase in pore water pressure in the vicinity of the line of injection. Within < 1 min, the vertical displacement increased rapidly, resulting in a slope failure after ~ 3 min.

Once the constant-head tank was hydraulically connected to the system, the piezometer showed a sudden drop in head. This might indicate that the tubing was not quite sufficient to supply the flow required to maintain a constant-head boundary condition underneath the foot of the slope. Simultaneously, all pore water pressure heads in the system experienced a rapid initial increase, but after a short period of time, the increase in heads ceased, followed by a slow decrease. During these head changes, the external load remained constant. This decrease in pore water pressure preceded the failure of the system by a short amount of time (~ 30 s) and, as in Case B, it was a clear signal of impending system failure. Shortly after slope failure, the pressure heads recovered and again showed the expected

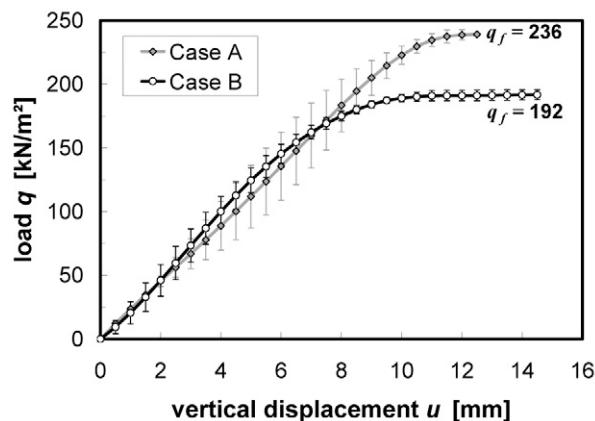


Fig. 8. Load–displacement diagram for Cases A (mean of Exp. A1–A5) and B (mean of Exp. B1–B3), ending with the load at slope failure (q_f).

value. Because these changes in head could not be due to flow, they had to be directly related to changes in the pore structure.

Discussion

Three sets of experiments were conducted. Each set was run at least in triplicate. The variability of the data shown in Table 2 was well in the acceptable range for experiments of this size; hence, reproducibility of the experiments may be assumed.

External load, water saturation, and flow dynamics (e.g., due to water injection) all potentially contribute to slope failure and their effects are strongly interdependent. Because the scope of this research primarily was to determine the effect of flow dynamics, saturation and external load were varied in the first two sets of experiments (Cases A and B) to determine suitable initial and boundary condition for Case C.

The hypothesis for the experiments was that an increase in pore water pressure could negatively affect the stability of a slope. Therefore, the first two sets of experiments were aimed at investigating the influence of water saturation and water pressure under static or steady-state conditions on the stability of a slope and, hence, to “set the stage” for the third set of experiments. Due to the size of the experiments and due to the capillary–pressure saturation curves for the sand used, it is a fair assumption that the water saturation in all experiments was very high. The difference was therefore less in the water saturation but rather in the corresponding capillary pressure.

In the first set of experiments (Case A), the groundwater table was located well below the expected shear band, while in Case B the groundwater level was raised into the expected shear band. It was demonstrated that a rise of the water table into the shear zone decreased the slope stability by 19%. This is a clear indication that capillary forces (even small ones for the given saturations) greatly contribute to the stability of a slope, much more so than actual water saturation values.

In the third set of experiments, water was injected and a transient water flow was introduced. Again it could be shown that the (pre-stressed) slope was stable as long as the capillary pressure in the vicinity of the shear band was greater than zero. A rise of the water table into the shear zone yielded an instant failure of the slope.

It is interesting to note that failure in each case was clearly preceded by a decrease in water head, followed by a drop when the slope collapsed. It may be assumed that the drop in pore water pressure during the visible failure was correlated to soil dilation, as described by Iverson et al. (2000). The gradual pressure decrease prior to failure shown here was also observed by Harp et al. (1990) in field experiments. A similar decrease in the pore water pressure before failure could also be seen in the numerical calculations by project partners (O. Avci, personal communication, 2009).

The capillary pressure–saturation curves for the sand in use are presented in Fig. 4. It has to be pointed out, though, that it was not always possible to exactly determine the saturation because it was affected by the hysteretic behavior of the sand. While the saturation in the experiments of Case A could be determined based on the primary drainage curve, the saturations for Cases B and C were harder to estimate because these experiments were conducted during or after an imbibition period.

For Case A, the initial water level was at 90 cm (all sand was fully saturated) and the water level was then lowered to 10 cm. Hence, the saturation above the resulting water level was on a drainage curve. The capillary pressure–saturation curves for the sand show an air-entry pressure of ~ 50 cm (Fig. 4). Hence we may assume that the soil was at near full saturation (capillary fringe) to a height of 60 cm. The top 30 cm in the experiment showed a fairly small saturation and, hence, a large surface of the interface between the wetting and nonwetting phases. We postulate that this condition positively affected the stability of the slope.

In the subsequent experiments (Cases B and C), the soil was initially drained as in Case A. For Case B, the left boundary was then raised to 70 cm while the water table on the right side remained fixed at 10 cm. It is a good assumption, therefore, that the saturations could be determined based on the primary imbibition curve. For Case C, both boundaries were fixed at 10 cm and there was an injection underneath the slope. The water flow was dynamic and the failure occurred fairly rapidly. It must be concluded, therefore, that the imbibition process was still active when the slope failed. Hence, for identical water pressures in Cases B and C, it has to be concluded that the saturation above the water table was smaller for Case C. This implies that the corresponding capillary suction was greater and, hence, the slope was more stable.

While all experiments were conducted with a fine, homogeneous sand, slopes in the “real world” are usually heterogeneous and they may contain an appreciable fraction of clay or silt, which will result in a different stability behavior. The sand for the experiment was selected because it showed a fairly small permeability, in order to approach natural permeabilities as much as possible. Its shear parameters were known and, hence, the results of this benchmark experiment could be directly used for the development and verification of numerical models. Transferring the results to different soils, of course, requires a primary knowledge of the respective soil parameters.

Regarding the scale of the experiments, three main issues were considered. In reality, slopes are of a much longer extent and hence the load to be sustained by the lower parts of the slope is much higher. We tried to imitate this with the use of external loads. Real slopes may be regarded as infinite in their extent along contour lines or, in other words, the friction along the sides of the slope may be neglected. The width selected for the experiment was limited by

the magnitude of the external load. Because this may not have been wide enough to fully neglect boundary conditions, after failure the shear plane was determined. Hence, possible friction along the sides may be accounted for in the three-dimensional numerical model. No attempt was made to change the effects of capillarity to fit the model because, in our opinion, all attempts in this regard would have been futile. Scaling issues were, hence, observed where possible; if an observation was not possible, the parameters of the experiment were chosen such that the experiments were still valid as benchmarks and could be used to validate numerical models.

Conclusions

Slope failure experiments on slopes built from homogeneous fine sands were conducted as benchmarks to obtain a better understanding of the slope physics and to provide sound data sets for project partners developing and validating numerical models. External load, saturation, and flow dynamics all have a distinct impact on slope stability or failure. In three sets of experiments, their effects were investigated. Case A (static water table underneath the foot of the slope) and Case B (steady-state flow conditions with a water table well within the expected shear zone) were conducted to delineate the influence of saturation on slope stability. It was shown that slopes stability was at a maximum when the shear zone was unsaturated (Case A). Once the water level was increased such that the water pressure in sections of the shear zone became positive (Case B), the slope failed at a much smaller external load. In the cases reported, the decrease in stability was about 19%. For the given fine-grained material in both cases (A and B), most of the shear zone was water saturated. While in Case A the pore water in the whole area was under negative pressure, in Case B it was partially under positive pressure. Therefore, it may be concluded that destabilization did not occur as a direct effect of saturation but rather as an effect of decreasing capillary. While it could be shown that capillary forces increase the stability of a slope and that the positive water pressure destabilizes the slope, the magnitude of the groundwater flow velocity had no or at most an insignificant effect on the slope stability.

The investigation of dynamic flow effects (Case C) showed that a system can be destabilized very easily if the water pressure and hence the buoyancy forces in the vicinity of the foot of the slope changes. Failure occurs as soon as the saturated zone with positive water pressure reaches the shear band. The sustained load for the case with a dynamic change in the water table was slightly higher than for the steady-state flow case. This may be explained by the hysteretic behavior of the capillary pressure curve, which resulted in higher capillary forces in the dynamic case and, hence, in a higher slope stability for an identical water table. Further investigation to quantify this effect is currently underway.

A very interesting observation was that each slope failure was preceded by a noticeable decrease in head. This means that even before

the failure was either visually observed or indicated in the pressure–deformation response, an internal relaxation of the system had to occur. This effect needs to be examined further. Eventually it might be possible to install a measuring system to monitor the pore water pressure in a real system. Correlating rapid changes in water pressure, changes that cannot be attributed to fluid flow, to measurements of slope movement may be a method to indicate slope stability.

While the primary goal of the experiments was to obtain benchmark data for further investigation of slope movements, scaling issues were, where possible, taken into account to ensure maximum transferability of the results. The experiments were conducted with sand; if soil parameters for other soils are known, however, the results can be transferred. The external loads imposed on the slope were implemented to simulate natural upslope pressures destabilizing a slope. In spite of the fact that water saturation is one of the main driving factors of slope failure, no attempt at scaling capillary pressure–saturation curves was made. Knowing the dependence of saturation and stability, these issues can be dealt with. The same holds true for heterogeneities and anisotropies, which cannot be neglected and may weaken or strengthen a slope. As for saturation, these soil parameters cannot be scaled in an experiment and need to be implemented in a numerical model.

While the experiments give good insight into parameters affecting slope stability, the effect of dynamic flow conditions needs to be further developed. In particular, this includes questions regarding a possible effect of the slope of the groundwater table for the steady-state case and the impact of the water injected at the foot of the slope.

Acknowledgments

Funding for this study was provided by the DFG (German Research Foundation) in the framework of the research unit “Coupling of Flow and Deformation Processes for Modeling the Movement of Natural Slopes.”

References

- Ahrenholz, B., J. Tölke, P. Lehmann, A. Peters, A. Kaestner, M. Krafczyk, and W. Durner. 2008. Prediction of capillary hysteresis in a porous material using lattice-Boltzmann methods and comparison to experimental data and a morphological pore network model. *Adv. Water Resour.* 31:1151–1173.
- Bathurst, R.J., J.A. Blatz, and M.H. Buger. 2003. Performance of instrumented large-scale unreinforced and reinforced embankments loaded by a strip footing to failure. *Can. Geotech. J.* 40:1067–1083.
- Cho, S.E., and S.R. Lee. 2001. Instability of unsaturated soil slopes due to infiltration. *Comput. Geotech.* 28:185–208.
- Crosta, G.B., and P. Frattini. 2008. Rainfall-induced landslides and debris flows. *Hydrol. Processes* 22:473–477.
- Durner, W., E.B. Schultze, and T. Zurmühl. 1997. State-of-the-art in inverse modeling of inflow/outflow experiments. p. 661–681. *In* M.Th. van Genuchten et al. (ed.) *Characterization and measurement of the hydraulic properties of unsaturated porous media*. Proc. Int. Worksh., Riverside, CA. 22–24 Oct. 1997. Univ. of California, Riverside.
- Ehlers, W., O. Avci, and B. Markert. 2011. Computation of slope movements initiated by rain-induced shear bands in small-scale tests and in situ. *Vadose Zone J.* 10:512–525, doi:10.2136/vzj2009.0156 (this issue).
- Ehlers, W., T. Graf, and M. Ammann. 2004. Deformation and localization analysis of partially saturated soil. *Comput. Methods Appl. Mech. Eng.* 193:2885–2910.
- El Sawwaf, M.A. 2007. Behavior of strip footing on geogrid-reinforced sand over a soft clay slope. *Geotext. Geomembranes* 25:50–60.

- Germer, K., and J. Braun. 2009. Slope failure processes in a laboratory flume. p. 115–118. *In* J.-P. Malet et al. (ed.) *Landslide processes: From geomorphological mapping to dynamic modelling*. CEREG Ed., Strasbourg, France.
- Harp, E.L., W.G. Wells II, and J.G. Sarmiento. 1990. Pore pressure response during failure in soils. *Geol. Soc. Am. Bull.* 102:428–438.
- Huang, C.-C., Y.-J. Ju, L.-K. Hwu, and J.-L. Lee. 2009. Internal soil moisture and piezometric responses to rainfall-induced shallow slope failures. *J. Hydrol.* 370:39–51.
- Huang, C.-C., C.-L. Lo, J.-S. Jang, and L.-K. Hwu. 2008. Internal soil moisture response to rainfall-induced slope failures and debris discharge. *Eng. Geol.* 101:134–145.
- Huang, C.-C., F. Tatsuoka, and Y. Sato. 1994. Failure mechanisms of reinforced sand slopes loaded with a footing. *Soils Found.* 34:27–40.
- Iverson, R.M., M.E. Reid, N.R. Iverson, R.G. LaHusen, M. Logan, J.E. Mann, and D.L. Brien. 2000. Acute sensitivity of landslide rates to initial soil porosity. *Science* 290:513–516.
- Iverson, R.M., M.E. Reid, and R.G. LaHusen. 1997. Debris-flow mobilization from landslides. *Annu. Rev. Earth Planet. Sci.* 25:85–138.
- Laouafa, F., and F. Darve. 2002. Modelling of slope failure by a material instability mechanism. *Comput. Geotech.* 29:301–325.
- Li, X., Z. Liu, R.W. Lewis, and K. Suzuki. 2003. Mixed finite element method for saturated poroelastoplastic media at large strains. *Int. J. Numer. Methods Eng.* 57:875–898.
- Lindenmaier, F., E. Zehe, A. Dittfurth, and J. Ihringer. 2005. Process identification at a slow moving landslide in the Vorarlberg Alps. *Hydrol. Processes* 19:1635–1651.
- Lorentz, S.A., D.S. Durnford, and A.T. Corey. 1992. Liquid retention measurements in porous media using a controlled outflow cell. *Dep. of Chem. and Bioresour. Eng., Colorado State Univ., Fort Collins.*
- Lourenço, S.D.N., K. Sassa, and H. Fukuoka. 2006. Failure process and hydrologic response of a two layer physical model: Implications for rainfall-induced landslides. *Geomorphology* 73:115–130.
- Moriwaki, H., T. Inokuchi, T. Hattanji, K. Sassa, H. Ochiai, and G. Wang. 2004. Failure processes in a full-scale landslide experiment using a rainfall simulator. *Landslides* 1:277–288.
- Okura, Y., H. Kitahara, H. Ochiai, T. Sammori, and A. Kawanami. 2002. Landslide fluidization process by flume experiments. *Eng. Geol.* 66:65–78.
- Olivares, L., and E. Damiano. 2007. Postfailure mechanics of landslides: Laboratory investigation of flowslides in pyroclastic soils. *J. Geotech. Geoenviron. Eng.* 133:51–62.
- Paul, D.K., and S. Kumar. 1997. Stability analysis of slope with building loads. *Soil Dyn. Earthquake Eng.* 16:395–405.
- Peters, A., and W. Durner. 2008. Simplified evaporation method for determining soil hydraulic properties. *J. Hydrol.* 356:147–162.
- Rahardjo, H., T.T. Lee, E.C. Leong, and R.B. Rezaur. 2005. Response of a residual soil slope to rainfall. *Can. Geotech. J.* 42:340–351.
- Roy, S., and N. Mandal. 2009. Modes of hill-slope failure under overburden loads: Insights from physical and numerical models. *Tectonophysics* 473:324–340.
- Tohari, A., M. Nishigaki, and M. Komatsu. 2007. Laboratory rainfall-induced slope failure with moisture content measurement. *J. Geotech. Geoenviron. Eng.* 133:575–587.
- Tsagaras, I., H. Rahardjo, D.G. Toll, and E.C. Leong. 2003. Infiltration characteristics of two instrumented residual soil slopes. *Can. Geotech. J.* 40:1012–1032.
- van Genuchten, M.Th. 1980. A closed-form equation for predicting the hydraulic conductivity of unsaturated soils. *Soil Sci. Soc. Am. J.* 44:892–898.
- Wang, G., and K. Sassa. 2001. Factors affecting rainfall-induced flowslides in laboratory flume tests. *Geotechnique* 51:587–599.
- Wang, G., and K. Sassa. 2003. Pore-pressure generation and movement of rainfall-induced landslides: Effects of grain size and fine-particle content. *Eng. Geol.* 69:109–125.
- Wang, F., and H. Shibata. 2007. Influence of soil permeability on rainfall-induced flowslides in laboratory flume tests. *Can. Geotech. J.* 44:1128–1136.
- Wienhöfer, J., K. Germer, F. Lindenmaier, A. Färber, and E. Zehe. 2009. Applied tracers for the observation of subsurface stormflow at the hillslope scale. *Hydrol. Earth Syst. Sci.* 13:1145–1161.
- Yoo, C. 2001. Laboratory investigation of bearing capacity behavior of strip footing on geogrid-reinforced sand slope. *Geotext. Geomembranes* 19:279–298.
- Zurmühl, T. 1996. Evaluation of different boundary conditions for independent determination of hydraulic parameters using outflow methods. p. 165–184. *In* P. DuChateau and J. Gottlieb (ed.) *Parameter identification and inverse problems in hydrology, geology and ecology*. Water Sci. Technol. Libr. 23. Kluwer Acad. Press, Dordrecht, the Netherlands.
- Zurmühl, T. 1998. Capability of convection dispersion transport models to predict transient water and solute movement in undisturbed soil columns. *J. Contam. Hydrol.* 30:99–126.